Mon. Not. R. Astron. Soc. **000**, 000–000 (0000) Printed 24 October 2014 (MN LATEX style file v2.2)

Early flattening of dark matter cusps in dwarf spheroidal galaxies

Carlo Nipoti[1⋆] and James Binney[2]
[1] *Department of Physics and Astronomy, Bologna University, viale Berti-Pichat 6/2, I-40127 Bologna, Italy*
[2] *Rudolf Peierls Centre for Theoretical Physics, Keble Road, Oxford OX1 3NP, UK*

arXiv:1410.6169v1 [astro-ph.GA] 22 Oct 2014

Accepted 2014 October 22. Received 2014 October 3; in original form 2014 June 17

ABSTRACT
Simulations of the clustering of cold dark matter yield dark-matter halos that have central density cusps, but observations of totally dark-matter dominated dwarf spheroidal galaxies imply that they do not have cuspy central density profiles. We use analytic calculations and numerical modelling to argue that whenever stars form, central density cusps are likely to be erased. Gas that accumulates in the potential well of an initially cuspy dark-matter halo settles into a disc. Eventually the surface density of the gas exceeds the threshold for fragmentation into self-gravitating clouds. The clouds are massive enough to transfer energy to the dark-matter particles via dynamical friction on a short time-scale. The halo's central cusp is heated to form a core with central logarithmic density slope $\gamma \approx 0$ before stellar feedback makes its impact. Since star formation is an inefficient process, the clouds are disrupted by feedback when only a small fraction of their mass has been converted to stars, and the dark matter dominates the final mass distribution.

Key words: dark matter – galaxies: dwarf – galaxies: evolution – galaxies: formation – instabilities

1 INTRODUCTION

The observed stellar velocity dispersions of dwarf spheroidal galaxies (dSphs) cannot be explained by assuming that the stars are in equilibrium in a gravitational potential dominated by the baryons: the standard interpretation of the observed stellar kinematics is that the mass distribution of dSphs is everywhere dominated by dark matter (DM), with mass to light-ratios $M/L \approx 10 - 100(M/L)_\odot$ (Aaronson 1983; Faber & Lin 1983; Mateo 1998). This property makes dSphs natural laboratories to study the density distribution of DM halos. However, although most observational studies agree that DM dominates over baryons even within the half-light radius (e.g. Strigari et al. 2008; Walker et al. 2009; Battaglia, Helmi, & Breddels 2013; Collins et al. 2014), it is still debated whether the inner distribution of DM is characterized by a cusp or a core (e.g. Breddels & Helmi 2013; Jardel et al. 2013). A consensus is emerging that the best observations disfavour the presence of steep central DM cusps such as those predicted by cosmological N-body simulations in a concordance Λ cold dark matter universe (Battaglia et al. 2008; Walker & Peñarrubia 2011; Agnello & Evans 2012; Amorisco, Agnello, & Evans 2013).

Our understanding of the process of formation of dSphs is still far from complete. In the most popular scenario dSphs formed originally as gas rich dwarf irregular or disc galaxies and then lost their gas as a consequence of internal or environmental effects (e.g. Lin & Faber 1983; Mayer et al. 2001, 2006; Milosavljević & Bromm 2014, and references therein). A successful formation model should be able to account for the all the properties of dSphs that can be inferred from observations, such as the structure and kinematics of the stellar distribution, metallicity of stars, and star formation history. Several studies have been carried out trying to reproduce at least some of these properties with either cosmological hydrodynamical simulations (Sawala et al. 2010; Sawala, Scannapieco, & White 2012; Simpson et al. 2013), simulations of isolated halos (Revaz et al. 2009; Assmann et al. 2013) or semi-analytic models (Li, De Lucia, & Helmi 2010; Font et al. 2011; Romano & Starkenburg 2013; Starkenburg et al. 2013). Here we focus on the two specific properties of dSphs: the facts that DM dominates the mass budget throughout these galaxies and that the present-day DM profile is not divergent in the central regions.

Several mechanisms are likely to jointly determine the DM distribution of dSphs: baryon removal by supernova feedback or ram pressure (Navarro, Eke, & Frenk 1996; Read & Gilmore 2005; Zolotov et al. 2012; Arraki et al. 2014), clumpy baryonic infall (El-Zant, Shlosman, & Hoffman 2001; Goerdt et al. 2010; Cole, Dehnen, & Wilkinson 2011) and stellar-feedback driven fluctuations of the gravitational potential (Mashchenko, Couchman, & Wadsley 2006; Mashchenko, Wadsley, & Couchman 2008). This last mechanism has recently drawn the attention of several authors who explored its feasibility within a cosmological framework (Governato et al. 2012; Garrison-Kimmel et al. 2013; Amorisco, Zavala, & de Boer 2014; Madau, Shen, & Governato 2014). However, given the uncertainties on the physics of stellar feedback, it is unclear whether the properties of present-day dSphs can be explained by the associated gravitational potential fluctuations (Peñarrubia et al. 2012; Pontzen & Governato 2014). Here we ar-

⋆ E-mail: carlo.nipoti@unibo.it

© 0000 RAS

gue that in the progenitors of dSphs the distribution of DM was substantially affected by baryons *before* star formation got underway, because in these systems star formation is inevitably preceded by the formation of massive baryonic clumps. The orbital decay of these clumps erased the central cusps of their host halos.

We present a coherent picture that leads from the cosmological DM halo to the matter distribution of a present-day dSph, taking as reference objects the classical dSphs of the Milky-Way. We do not attempt to simulate self-consistently the entire formation and evolution process, but we focus on the most important steps, demonstrating quantitatively that the proposed picture is feasible.

We envisage the following scenario for the formation and early evolution of the baryonic and dark components of dSphs.

(i) The host DM halo is initially cuspy as predicted by cosmological *N*-body simulations.
(ii) Gas accumulates in the halo potential well and settles into a disc.
(iii) The infall of gas initially tends to make the halo cuspier, but the effect is small as long as the gas density is lower than the DM density.
(iv) Once the gas density becomes higher than the local DM density, the gas disc becomes unstable and starts to fragment.
(v) Since the gas temperature is not negligible with respect to the system virial temperature, the disc fragments into large clumps of gas.
(vi) These big clumps transfer energy to the DM particles via dynamical friction: the halo is quickly heated and the central cusp is flattened into a core.
(vii) Subsequently, stars start to form in the clumps, and efficient stellar feedback then expels most of the gas, so the final stellar density is much lower than both the initial gas density and the final DM density.

The aim of this work is to give a quantitative description of the main physical processes involved in the above scenario, focusing in particular on demonstrating that fragmentation occurs where baryons are dominant (iv), that the resulting gas clumps are very massive (v), and that these clumps quickly flatten the original DM cusp (vi). As mentioned above, the idea that the DM profiles of dSphs are flattened by baryonic clumps has been considered in other works (El Zant et al. 2001; Goerdt et al. 2010; Cole et al. 2011). Here we put this proposal into a broader context by modelling the coevolution of DM and baryons in dSphs starting from cosmic gaseous accretion and estimating self-consistently the properties of the gaseous clumps responsible for the flattening of the DM density profile.

The paper is organized as follows. In Section 2 we define the properties of the protogalaxy model. Section 3 discusses the coevolution of baryons and DM. In Section 4 we relate our work to previous work on the subject. Section 5 concludes.

2 PROTOGALAXY MODEL

2.1 Dark matter halo

We assume that the DM halo is represented initially by a spherical Navarro, Frenk, & White (1995, NFW) distribution with density

$$\rho_{\rm DM}(r) = \frac{\rho_{\rm DM,0}}{(r/r_{\rm s})(1+r/r_{\rm s})^2} \tag{1}$$

and gravitational potential

$$\Phi_{\rm DM}(r) = -4\pi G\rho_{\rm DM,0}{r_{\rm s}}^2\frac{\ln(1+r/r_{\rm s})}{r/r_{\rm s}}, \tag{2}$$

where

$$\rho_{\rm DM,0} \equiv \frac{200}{3}\frac{\rho_{\rm crit}c_{200}^3}{\ln(1+c_{200})-c_{200}/(1+c_{200})}. \tag{3}$$

Here $r_{\rm s}$ is the scale radius, $c_{200} \equiv r_{\rm s}/r_{200}$ is the concentration and r_{200} is the virial radius. The critical density of the Universe $\rho_{\rm crit}(z) = 3H^2(z)/8\pi G$ depends on redshift z through the Hubble parameter

$$H(z) = H_0\left[\Omega_{m,0}(1+z)^3+\Omega_{\Lambda,0}\right]^{1/2}, \tag{4}$$

where H_0 is the Hubble constant, and $\Omega_{\rm m,0}$ and $\Omega_{\Lambda,0}$ are the present-day normalized densities of matter and dark energy. We assume $H_0 = 70\,{\rm km\,s^{-1}\,Mpc^{-1}}$, $\Omega_{\Lambda,0} = 0.73$ and $\Omega_{\rm m,0} = 0.27$.

In this work we focus on classical dSphs, such as the Milky-Way satellites Fornax and Scupltor, having DM halos with masses of the order of $10^9 M_\odot$. These objects likely formed in lower density environments at $z \sim 2$, because dwarf galaxies that formed at much higher redshift will have done so in dense environments, and merged into more massive systems by $z \sim 0$. Given a halo mass and redshift, the concentration c_{200} can be estimated from cosmological *N*-body simulations (e.g. Muñoz-Cuartas et al. 2011; Prada et al. 2012; Ogiya et al. 2014; Ishiyama et al. 2013). For our reference halo model we fix $z = 2$, $M_{\rm DM} = 10^9 M_\odot$, $c_{200} = 5.69$, so the virial radius is $r_{200} \simeq 10.3\,{\rm kpc}$ and the scale radius is $r_{\rm s} \simeq 1.81\,{\rm kpc}$.

2.2 Gas temperature

In the first stages of galaxy formation gas will fall into the halo potential well. In the considered case the halo is located in a low-density environment, so the infalling gas should be either primordial or very metal poor. It is often assumed that such gas is shock heated to the halo virial temperature

$$T_{\rm vir} \equiv \frac{\mu m_{\rm p}}{2k_{\rm B}}\frac{GM_{\rm DM}}{r_{200}}, \tag{5}$$

where μ is the mean mass per particle in units of the proton mass $m_{\rm p}$. For our reference halo ($M_{\rm DM} = 10^9 M_\odot$, $z = 2$) we get $T_{\rm vir} \simeq 1.49\times10^4\,{\rm K}$ with $\mu = 0.6$, but in practice most of the gas is gas is less strongly heated than this (Binney 1977; Birnboim & Dekel 2003), so $10^4\,{\rm K}$ is a conservative upper limit on the temperature of the gas. The ability of gas to cool below $10^4\,{\rm K}$ crucially depends on the gas metallicity, on the fraction of molecular hydrogen and on the presence of a background radiation field (see, e.g., Stiavelli 2009, Loeb & Furlanetto 2013 and reference therein). Rather than attempting to model in detail the cooling process below $T = 10^4\,{\rm K}$, we consider two representative cases: one in which cooling is more effective, and the gas temperature is $T = 3\times10^2\,{\rm K}$ (model T2) and the other in which cooling is less effective and the gas temperature is $T = 3\times10^3\,{\rm K}$ (model T3).

2.3 Disc instability

In the presence of angular momentum the infalling and cooling gas is expected to settle into a disc. At low gas density the disc is stable, but above a critical density the disc becomes gravitationally unstable and fragments. We are therefore interested in determining the physical conditions for the onset of such instability. For infinitesimally thin gaseous disks such conditions are determined by Toomre's stability criterion (Safronov 1960; Toomre 1964). A priori it is not obvious that the thin-disc approximation is appropriate in the considered case. If the gas temperature T is much lower than $T_{\rm vir}$ the disc is thin, but the thickness of the disc is not negligible if T is a significant fraction of $T_{\rm vir}$. In any case, we proceed under

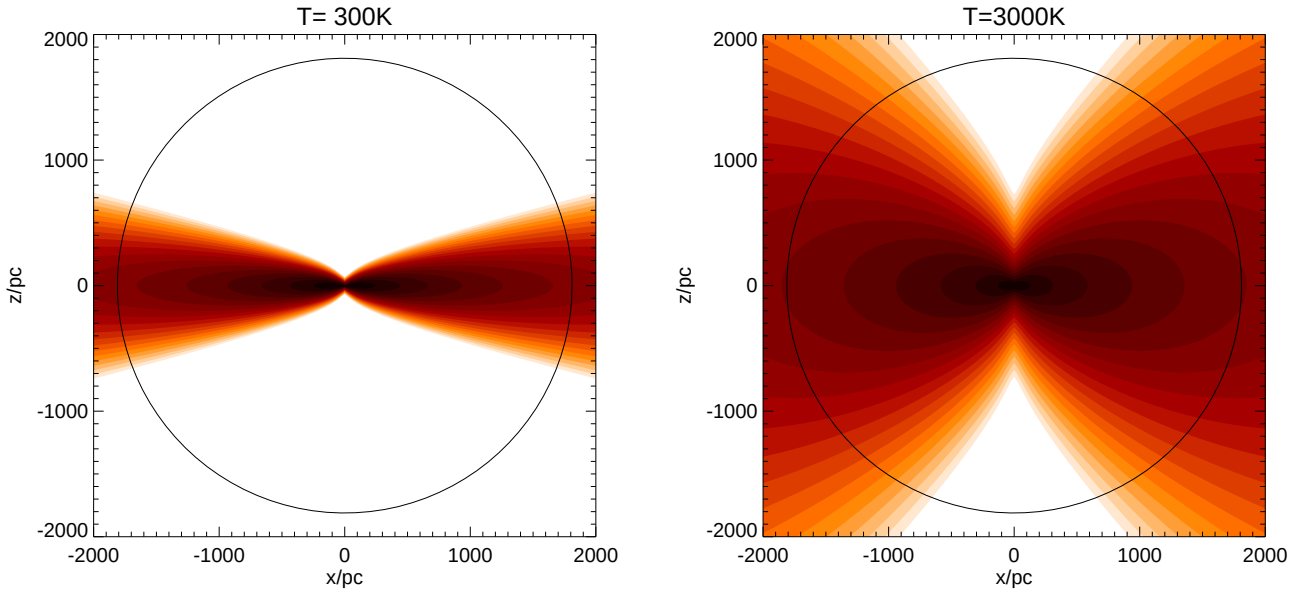

Figure 1. Gas iso-density contours (logarithmically spaced by 0.5 dex) in the meridional plane of models T2 (left-hand panel) and T3 (right-hand panel). Contours corresponding to densities lower than the maximum gas density by more than 10 orders of magnitude are not shown. In each panel the circle indicates the DM halo scale radius r_s.

Table 1. Parameters of the models T2 and T3. T: gas temperature. $M_{\rm gas}$: total gas mass. $f_{\rm v} \equiv \Omega R/v_{\rm circ}$: normalization of the rotation law. $\lambda_{\rm inst}$: wavelength of the fastest-growing mode (equation 8). $R_{\rm inst}$: radius at which the instability occurs. $h_{\rm z,inst}$: vertical scale-height at $R_{\rm inst}$. $M_{\rm inst}$: mass corresponding to the fastest-growing unstable mode (equation 9). The DM halo is the same in both models (see Section 2.1).

Model	T/K	$M_{\rm gas}/M_\odot$	$f_{\rm v}$	$\lambda_{\rm inst}$/ pc	$R_{\rm inst}$/ pc	$\lambda_{\rm inst}/2\pi R_{\rm inst}$	$\lambda_{\rm inst}/h_{\rm z,inst}$	$M_{\rm inst}/M_\odot$
T2	3×10^2	1.168×10^7	0.9899	124.9	183.6	0.1083	7.275	1.541×10^5
T3	3×10^3	7.613×10^7	0.8938	484.0	240.5	0.3202	8.027	6.048×10^6

the assumption that the thin disc approximation is justified and we verify and discuss this hypothesis a posteriori.

Here we briefly recall the relevant equations for a local stability analysis of a self-gravitating gaseous disc (e.g. Binney & Tremaine 2008). The dispersion relation for a perturbation with wave-vector $\mathbf{k}$ is

$$\omega^2 = \kappa^2 - 2\pi G\Sigma_{\rm gas}k + v_{\rm s}^2k^2, \tag{6}$$

where ω is the perturbation frequency, $k = |\mathbf{k}|$ is the perturbation wave-number, $\Sigma_{\rm gas}$ is the local gas surface density, κ is the epicycle frequency and $v_{\rm s}$ is the adiabatic sound speed. The condition for disc stability ($\omega^2 > 0$ for all $\mathbf{k}$) can be written as $Q > 1$, where

$$Q \equiv \frac{v_{\rm s}\kappa}{\pi G\Sigma_{\rm gas}} \tag{7}$$

is Toomre's parameter. It can be shown that the same stability criterion holds also when the gas coexists with other matter, such as the DM halo: in this case the epicycle frequency κ is larger than that that generated by the gas on its own, and Q is higher at given gas surface density $\Sigma_{\rm gas}$. When $Q < 1$ the fastest growing mode is the one with $k = k_{\rm inst}$, where $k_{\rm inst}$ is such that $\mathrm{d}\omega^2/\mathrm{d}k = 0$, so $k_{\rm inst} = \pi G\Sigma_{\rm gas}/v_{\rm s}^2 = 2k_{\rm crit}/Q^2$, where $k_{\rm crit} \equiv \kappa^2/2\pi G\Sigma_{\rm gas}$ is the minimum unstable wave-number. The wavelength of the fastest-growing unstable mode is

$$\lambda_{\rm inst} = \frac{2\pi}{k_{\rm inst}} = \frac{2v_{\rm s}^2}{G\Sigma_{\rm gas}} = \frac{2\pi^2Q^2G\Sigma_{\rm gas}}{\kappa^2} = \frac{Q^2}{2}\lambda_{\rm crit}, \tag{8}$$

where $\lambda_{\rm crit} \equiv 4\pi^2G\Sigma_{\rm gas}/\kappa^2$ is the longest unstable wavelength. The mass corresponding to the fastest-growing unstable mode is

$$M_{\rm inst} = \pi\left(\frac{\lambda_{\rm inst}}{2}\right)^2\Sigma_{\rm gas}(R_{\rm inst}), \tag{9}$$

where $\Sigma_{\rm gas}(R_{\rm inst})$ is the gas density evaluated at the radius at which the instability occurs.

2.4 Gas distribution

Here we build three-dimensional axisymmetric disc models by computing an equilibrium solution for a body of isothermal gas that rotates differentially with angular velocity Ω in the total gravitational potential $\Phi = \Phi_{\rm DM} + \Phi_{\rm gas}$, where $\Phi_{\rm DM}$ (equation 2) and $\Phi_{\rm gas}$ are the gravitational potentials of DM and gas, respectively. We work in cylindrical coordinates (R, z). The momentum equation for isothermal gas at temperature T can be written

$$\frac{k_{\rm B}T}{\mu m_{\rm p}}\frac{\nabla\rho_{\rm gas}}{\rho_{\rm gas}} = -\nabla\Phi_{\rm eff}, \tag{10}$$

where $\rho_{\rm gas}$ is the gas density and

$$\Phi_{\rm eff}(R,z) = \Phi(R,z) - \int^R \mathrm{d}R'\,R'\Omega^2(R') \tag{11}$$

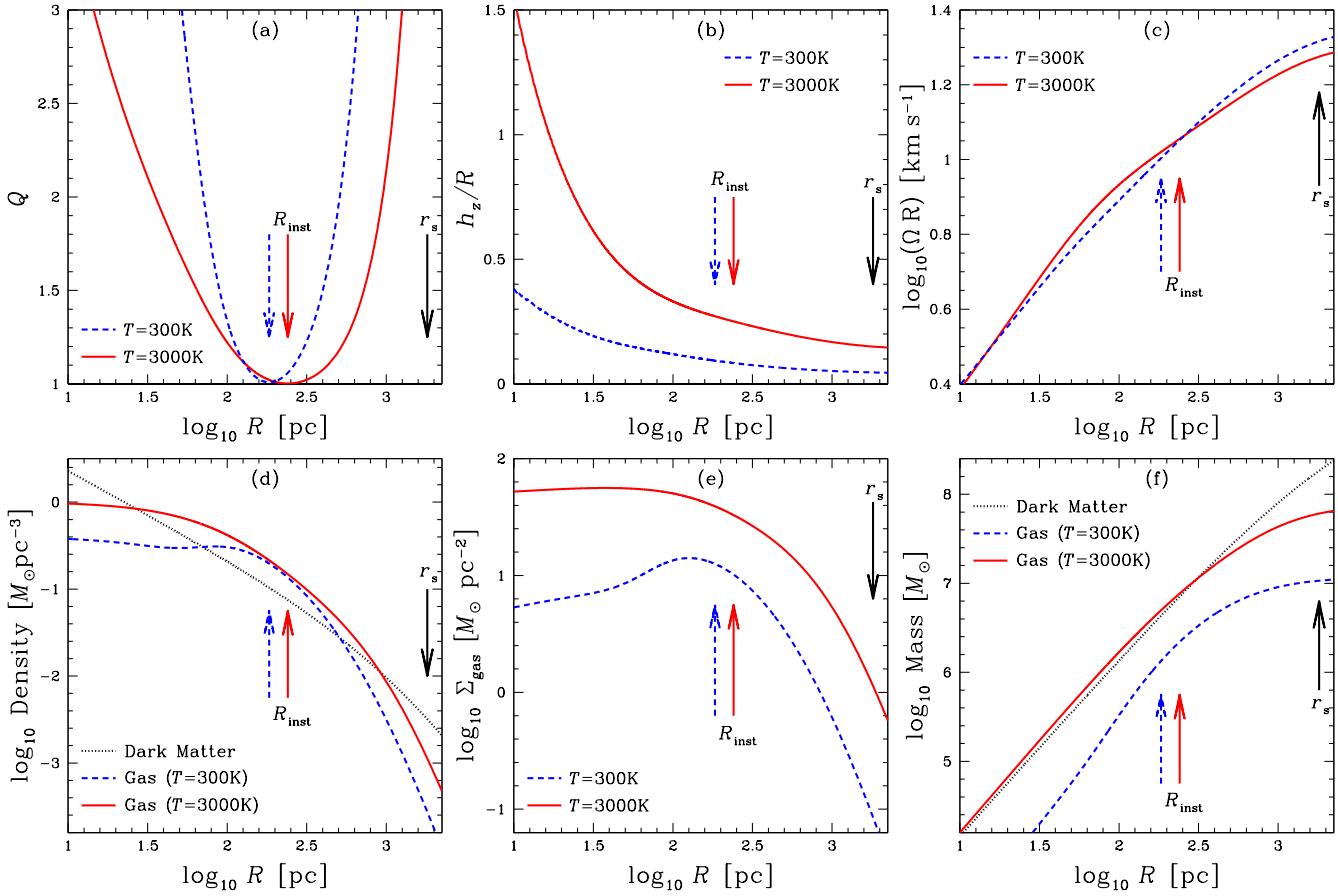

Figure 2. Radial profiles of Q parameter (panel a), vertical scale-height h_z (panel b), gas rotation speed (panel c), gas density at $z = 0$ (panel c), gas surface density (panel e) and gas mass (panel f) for models T2 ($T = 300$ K; dashed curves) and T3 ($T = 3000$ K; solid curves). In panels (d) and (f) the density and mass profiles of the DM halo are shown for comparison (dotted curves). The arrows indicate the gas instability radius $R_{\rm inst}$ and the halo scale radius $r_{\rm s}$.

is the effective potential. It follows that the density distribution is given by

$$\rho_{\rm gas}(R,z) \equiv \rho_{\rm gas,0}\,\exp\left\{-\frac{\mu m_{\rm p}}{k_{\rm B}T}\left[\Phi_{\rm eff}(R,z)-\Phi_{\rm eff,0}\right]\right\}, \qquad (12)$$

where $\rho_{\rm gas,0}$ and $\Phi_{\rm eff,0}$ are the density and effective potential at a reference point. We assume rotation law

$$\Omega(R) = f_{\rm v}\frac{v_{\rm circ}(R)}{R}, \qquad (13)$$

where $f_{\rm v} < 1$ is a dimensionless factor and $v_{\rm circ}$ is the circular speed of the total (DM plus gas) distribution measured in the equatorial plane, which is defined by

$$\frac{v_{\rm circ}^2}{R} = \frac{{\rm d}\Phi(R,0)}{{\rm d}R}, \qquad (14)$$

where $\Phi(R,z)$ is the total gravitational potential in cylindrical coordinates. The spherical halo potential is given analytically by equation (2). The gravitational potential of the gaseous disc $\Phi_{\rm gas}$ is computed numerically using the spherical harmonics-based solver of the Poisson equation contained in the numerical code N-MODY (Ciotti, Londrillo & Nipoti 2006; Londrillo & Nipoti 2009). As the gas distribution and velocity field depend on the gas potential and vice-versa, we find a solution iteratively computing $\Phi_{\rm gas}$, $\rho_{\rm gas}$ and $v_{\rm circ}$ up to convergence.

It is useful to define the face-on surface density of the disc

$$\Sigma_{\rm gas}(R) = 2\int_0^\infty {\rm d}z\,\rho_{\rm gas}(R,z) \qquad (15)$$

and the vertical scale height of the distribution $h_{\rm z}(R)$ such that

$$\int_R^{R+\Delta R}{\rm d}R'\int_0^{h_z}{\rm d}z'\,\rho_{\rm gas}(R',z') = \frac{1}{2}\int_R^{R+\Delta R}{\rm d}R'\int_0^{\infty}{\rm d}z'\,\rho_{\rm gas}(R',z'), \qquad (16)$$

i.e., $h_{\rm z}(R)$ is a measure of the thickness at radius R containing half of the mass in a cylindrical shell of radius R and width $\Delta R \ll R$.

For our three-dimensional disc models, the parameter Q (equation 7) can be computed at any R by combining $\Sigma_{\rm gas}(R)$ as given by equation (15), the local epicyclic frequency $\kappa(R)$, defined by

$$\kappa^2(R) = 4\Omega^2 + 2\Omega R\frac{{\rm d}\Omega}{{\rm d}R}, \qquad (17)$$

and the adiabatic sound speed $v_{\rm s} = 5k_{\rm B}T/3\mu m_{\rm p}$, which is independent of radius for the considered isothermal models.

2.5 Marginally stable disc models

We consider a scenario in which the gas accumulates from low densities (high Q) up to values of $\Sigma_{\rm gas}$ such that the Q-parameter reaches the value $Q = 1$ at some radius $R_{\rm inst}$, which is the radius at which the the fastest instability occurs. This fixes the gas surface

density normalization and thus $\rho_{\rm gas,0}$ appearing in equation (12). These "marginally stable" models are representative of the physical conditions of gaseous discs just before they fragment.

Here we present two representative marginally stable isothermal disc models in equilibrium in the common potential of the disc itself and of the NFW halo described in Section 2.1: model T2 ($T = 3\times10^2$ K) and model T3 ($T = 3\times10^3$ K). Here we adopt $\mu = 1.2$, as appropriate for primordial or very low-metallicity gas, which is mostly neutral at the considered temperatures and densities (e.g. Loeb & Furlanetto 2013). For given gas temperature, we assume $f_{\rm v} = \sqrt{1-T/T_{\rm vir}}$, so $f_{\rm v} \approx 1$ (maximum rotation) for $T \ll T_{\rm vir}$ and $f_{\rm v} \approx 0$ (no rotation) for $T \approx T_{\rm vir}$. The values of the parameters for models T2 and T3 are reported in Table 1.

Figure 1 shows the maps of the density distributions in the meridional plane for models T2 and T3. In both cases the density distribution is toroidal: the density contours appear like a flaring disc when the temperature is lower (model T2) and tend to be peanut-shaped at higher temperatures (model T3). In Fig. 2 we show, for the same two models, the radial profile of the Q parameter, the ratio h_z/R that measures the thickness of the disc, the rotation speed ΩR, the densities of gas and DM, the surface density of gas $\Sigma_{\rm gas}$, and the masses of gas and DM $M(R)$. By construction $Q \geq 1$ and $Q \simeq 1$ only at $R_{\rm inst}$ (Fig. 2a). The values of h_z/R suggest that the disc can be considered relatively thin over most of the gas mass distribution, and in particular $h_z/R \lesssim 0.3$ at $R_{\rm inst}$ (Fig. 2b). The shape of the speed profiles (Fig. 2c) are similar to the circular speed profile of the underlying NFW DM halo, with only slight differences due to the gravitational potential of the gas: the speed varies approximately as $R^{0.5}$ at small radii but flattens at larger radii. The profiles of $\rho_{\rm gas}$ and $\rho_{\rm DM}$ support the idea that the condition $\rho_{\rm gas} > \rho_{\rm DM}$ is required for fragmentation (Fig. 2d). The corresponding critical surface density for instability is $10-40 M_\odot\,{\rm pc}^{-2}$ (Fig. 2e). The total gas mass contained within $R = r_{200}$ is $M_{\rm gas} \simeq 1.2\times10^7 M_\odot$ (model T2) and $M_{\rm gas} \simeq 7.6\times10^7 M_\odot$ (model T3), much less than the total DM mass $M_{\rm DM} = 10^9$. However, the gas surface density drops abruptly at large radii: most ($\approx 90\%$ for model T2, $\approx 80\%$ for model T3) of the gas mass lies within $r_{\rm s}$, while only 13% of the DM mass ($1.3\times10^8 M_\odot$) is contained within $r_{\rm s}$ (Fig. 2f).

For self-consistency we must have $k_{\rm inst}R_{\rm inst} \gg 1$ (i.e. $\lambda_{\rm inst}/2\pi R_{\rm inst} \ll 1$) and $\lambda_{\rm inst}/h_{\rm z,inst} \gg 1$, where $h_{\rm z,inst} \equiv h_z(R_{\rm inst})$ is the vertical scale height of the disc at $R_{\rm inst}$. The wavelength $\lambda_{\rm inst}$ of the fastest growing unstable mode at this radius is reported in Table 1: we note that $\lambda_{\rm inst}/2\pi R_{\rm inst} \lesssim 0.3$ and $\lambda_{\rm inst}/h_{\rm z,inst} \gtrsim 7.3$, so the short-wavelength and thin-disc approximations, on which the stability analysis is based, are justified. The mass of the fastest-growing unstable mode (equation 9) is $M_{\rm inst} \approx 1.54\times10^5 M_\odot$ for model T2 and $M_{\rm inst} \approx 6.05\times10^6 M_\odot$ for model T3.

3 COEVOLUTION OF BARYONS AND DARK MATTER

3.1 Time-scales

The results of cosmological N-body simulations suggest that before gas infall the DM halo is cuspy (Navarro, Frenk, & White 1995). During gas infall the halo tends to contract (Blumenthal et al. 1986), but the effect is small as long as the gas density is lower than the DM density. When the gas density becomes comparable to or larger than the DM density, it is typically high enough to trigger Toomre's instability, so the gas disc starts to fragment into clumps. The mass of these clumps is $M_{\rm clump} \approx M_{\rm inst}$, where $M_{\rm inst}$ is the mass associated with the fastest growing unstable mode (equation 9).

When orbiting through the distribution of the much lighter DM particles, the massive clumps experience dynamical friction and therefore tend to spiral in towards the halo centre. The distribution of DM particles is heated by the energy transferred from the clumps, so the initial cosmological cusp of the DM halo is flattened by the clumps (e.g. El Zant et al. 2001). This process must happen on the dynamical friction time-scale, which, for a clump of mass $M_{\rm clump}$ in circular orbit at radius r is (Binney & Tremaine 2008, section 8.1)

$$t_{\rm fric} \simeq \frac{1.17}{\ln\Lambda}\frac{M_{\rm DM}(r)}{M_{\rm clump}}t_{\rm cross}, \qquad (18)$$

where $M_{\rm DM}(r)$ is the DM mass contained within r, $\ln\Lambda$ is the Coulomb logarithm and $t_{\rm cross} \equiv r/v_{\rm circ}$ is the crossing time. Applying the above formula to our reference models, fixing for instance $r = R_{\rm inst}$, we get $t_{\rm fric}/t_{\rm cross} \simeq 33/\ln\Lambda$ for model T2 (in which $t_{\rm cross} \approx 17$ Myr at $r = R_{\rm inst}$) and $t_{\rm fric}/t_{\rm cross} \simeq 1.4/\ln\Lambda$ for model T3 (in which $t_{\rm cross} \approx 21$ Myr at $r = R_{\rm inst}$). This suggests that, especially in the higher-temperature case, dynamical friction heating acts on a very short time-scale.

3.2 N-body simulations

To explore in detail the interaction between clumps and DM we ran N-body simulations. In each of these simulations the initial conditions consist of $N_{\rm clump}$ clumps of mass $M_{\rm clump}$ and softening length $\varepsilon_{\rm clump}$ on circular orbits in a spherical DM halo made of $N_{\rm DM} = 2\times10^6$ particles. In detail, the halo is represented by a truncated NFW distribution

$$\rho_{\rm DM}(r) = M_0\frac{\exp\left[-(r/r_{\rm t})^2\right]}{r\,(r+r_{\rm s})^2}, \qquad (19)$$

where $r_{\rm s} = 1.81$ kpc, $r_{\rm t} = 1.23 r_{200} \simeq 12.67$ kpc, and $M_0 \simeq 9.6\times10^8 M_\odot$: the values of these parameters are such that the central density profile coincides with that of the model described in Section 2.1 and the total DM mass is $M_{\rm DM} = 10^9 M_\odot$. We note that the DM mass within 300 pc is $1.1\times10^7 M_\odot$, consistent with observations of many dSphs (Strigari et al. 2008). Eddington's inversion (Binney & Tremaine 2008) is used to build the halo in equilibrium in its gravitational potential with isotropic velocity distribution. The gravitational potential of the clumps is neglected in setting up the halo: with this choice we implicitly include also the effect of contraction of the halo due to the presence of the baryons.

We present here results for two N-body simulations: simulation T2 with $M_{\rm clump} = 1.54\times10^5 M_\odot$, $N_{\rm clump} = 76$ and $\varepsilon_{\rm clump} = 63$ pc (based on model T2 in Section 2.5), and simulation T3 with $M_{\rm clump} = 6.05\times10^6 M_\odot$, $N_{\rm clump} = 12$ and $\varepsilon_{\rm clump} = 235$ pc (based on model T3 in Section 2.5). These values are such that $M_{\rm clump} \simeq M_{\rm inst}$, $\varepsilon_{\rm clump} \simeq \lambda_{\rm inst}/2$ and $N_{\rm clump}M_{\rm clump} \approx M_{\rm gas}$ (see Table 1). In the initial conditions all the clumps move tangentially within the equatorial plane $z = 0$. The initial radial distribution of the clumps follows the cumulative distribution function $f(R) = M_{\rm gas}(R)/M_{\rm gas}$ (see Fig. 2f). In practice, we first distribute $n = N_{\rm clump}/2$ clumps at radii R_i ($i = 1,\ldots,n$) such that $f(R_i) = \left(i-\frac{1}{2}\right)/n$, we extract the azimuthal angle ϕ_i from a uniform distribution in $[0,\pi]$ and we assign $v_{Ri} = 0$ and $v_{\phi_i} = \sqrt{GM_i/R_i}$, where $M_i \equiv M_{\rm DM}(R_i) + 2(i-1)M_{\rm clump}$, where $M_{\rm DM}(R_i)$ is the DM mass within $r = R_i$. The other n clumps are then given phase-space coordinates $R_i = R_{i-n}$, $\phi_i = \phi_{i-n} + \pi$, $v_{\phi_i} = v_{\phi_{i-n}}$ and $v_{Ri} = 0$ ($i = n+1,\ldots,N_{\rm clump}$), so that, even in the presence of the clumps, the centre of mass of the system is at rest in the centre of the DM distribution. The N-body simulations were run with the parallel collisionless code FVFPS (Londrillo, Nipoti, &

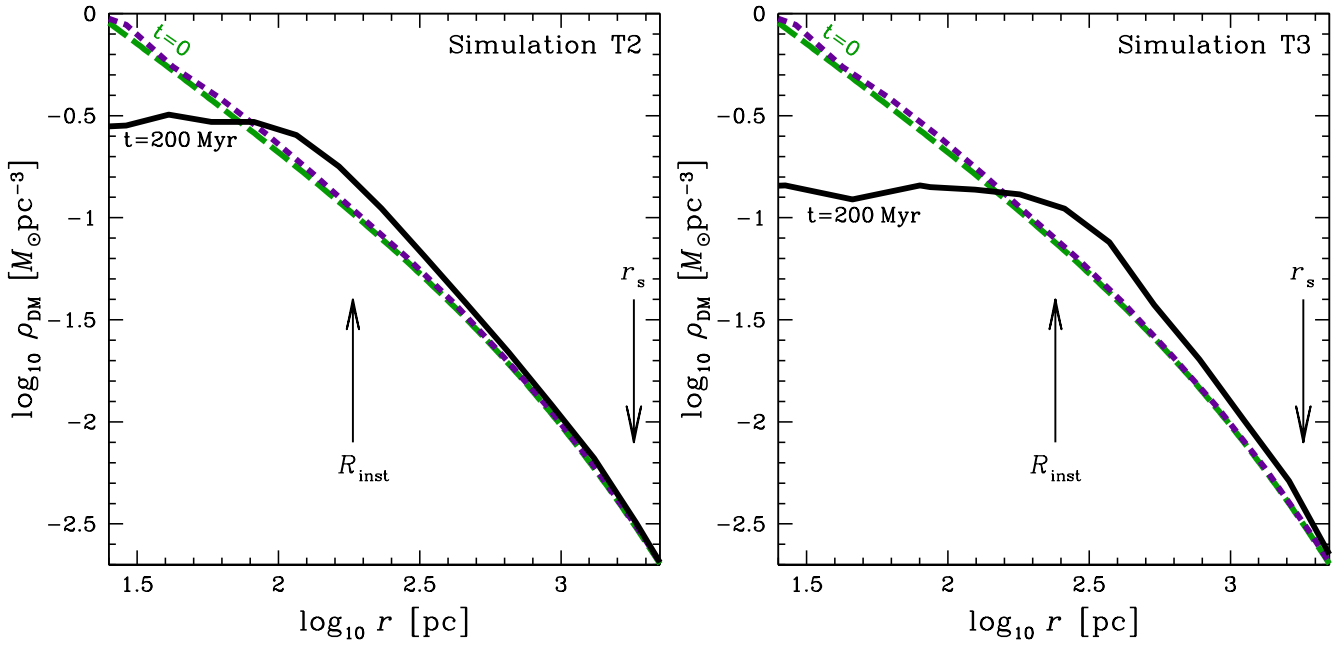

Figure 3. Initial ($t = 0$; long-dashed curves) and final ($t = 200$ Myr; solid curves) DM density profile in the presence of N_{clump} gas clumps of mass M_{clump} for models T2 (left-hand panel) and T3 (right-hand panel) as predicted by N-body simulations. In each panel the short-dashed curve is the profile obtained by letting the halo evolve in the absence of the clumps for 200 Myr.

Ciotti 2003; Nipoti, Londrillo, & Ciotti 2003). We adopted the following values of the code parameters: minimum value of the opening parameter $\theta_{min} = 0.5$, softening parameter for the DM particles $\varepsilon = 0.02 r_s = 36$ pc and time-step $\Delta t = 1.08$ Myr.

In both simulations T2 and T3 the effect of the presence of the clumps is to flatten the DM cusp and to produce a central core. The formation of the core is completed in ≈ 200 Myr in simulation T2 and ≈ 150 Myr in simulation T3, so we take $t = 200$ Myr as reference final snapshot. Figure 3 shows the DM profiles of the two simulations at $t = 0$ and $t = 200$ Myr. A comparison with the evolution of the halo in the absence of the clumps demonstrates that the core is not a numerical artifact (see Fig. 3). As expected, the effect is stronger in model T3 (higher gas temperature, more massive clumps) than in model T2 (lower gas temperature, less massive clumps). The final central logarithmic density slope $\gamma \equiv -\mathrm{d}\ln\rho_{DM}/\mathrm{d}\ln r$ is consistent with $\gamma = 0$ in both models, but the size of the core is significantly larger in simulation T3 (≈ 300 pc) than in simulation T2 (≈ 100 pc).

The final DM mass within 300 pc is $1.4 \times 10^7 M_\odot$ in simulation T2 and $1.3 \times 10^7 M_\odot$ in simulation T3, still consistent with the observational data (Strigari et al. 2008). The fact that the DM mass within 300 pc is higher than in the initial conditions ($1.1 \times 10^7 M_\odot$) is a consequence of the contraction of the halo due to the presence of the baryons. As mentioned above, in our experiments we implicitly account for the contraction of the halo because the halo is set up in equilibrium in its own gravitational potential, neglecting the potential of the clumps. The final profiles shown in Fig. 3 result from the combination of contraction due to baryonic infall and expansion due to dynamical friction heating. We verified with simple N-body experiments that if the same halo evolves in the absence of the clumps, but in the presence of a fixed gravitational potential representing the corresponding smooth gas distribution, the central DM profile quickly ($\lesssim 50$ Myr) settles into a new equilibrium configuration with slightly steeper central slope ($\gamma \simeq 1.1$ for model T2 and $\gamma \simeq 1.2$ for model T3) than the initial $\gamma = 1$. However, when the gas fragments into clumps, the slight steepening due to contraction is overwhelmed by heating through dynamical friction, and the final profiles are cored with $\gamma \approx 0$.

3.3 Lifetime of the gas clumps

For the mechanism described above to be effective, the lifetime of the gas clumps must be at least of the same order as the time ($\sim 10^8$ yr) necessary to redistribute the DM in the central regions of the halo. In general, the question of the evolution of massive clouds in galaxies is complex and highly debated, especially because it is strictly related to the poorly understood process of star formation and associated feedback (e.g. Murray, Quataert, & Thompson 2010; Genel et al. 2012; Hopkins, Quataert, & Murray 2012; Bournaud et al. 2014). However, in the specific context here considered, a few simple arguments suggest that the assumption of a long clump lifetime is a reasonable one.

It is widely accepted that any mechanism responsible for cloud disruption starts to act after the formation of the first stars. At $T \lesssim 10^4$ K metal-poor gas has difficulty cooling, especially in the absence of molecules, and molecules form with difficulty in the absence of dust. The time-scale for star formation cannot be shorter than the longer of the cloud's initial dynamical time $t_{dyn} = (G\rho_{gas})^{-1/2}$ and the cooling time $t_{cool} = 3k_B T/2\mathcal{L}f_{H_2}$, where $\mathcal{L} = \mathcal{L}(T, \rho_{gas})$ is the cooling rate per molecule and $f_{H_2} = n_{H_2}/n_{gas}$ is the molecular-hydrogen fraction (n_{H_2} is the molecular-hydrogen number density and $n_{gas} = \rho_{gas}/\mu m_p$ is the total gas number density). Taking as gas density $\rho_{gas}(R = R_{inst}, z = 0)$ and estimating $\mathcal{L}$ from equation 2.32 of Stiavelli (2009), for our models we get $t_{dyn} \simeq 3.4 \times 10^7$ yr and $t_{cool} \simeq 2.8 \times 10^9 (f_{H_2}/10^{-5})^{-1}$ yr when $T = 3 \times 10^2$ K, and $t_{dyn} \simeq 3.9 \times 10^7$ yr and $t_{cool} \simeq 1.5 \times 10^7 (f_{H_2}/10^{-5})^{-1}$ yr

when $T = 3 \times 10^3$ K. Notwithstanding the dependence of $t_{\rm cool}$ on the poorly constrained parameter $f_{\rm H_2}$, these numbers suggest that the star-formation time-scale should not be shorter than a few tens of megayears. Even when the first burst of star formation occurs, the cloud is not immediately shattered: if cloud disruption is due to supernovae, which however is controversial (Murray et al. 2010), $\sim 10^7$ yr from the onset of star formation is required for massive stars to complete their lives.

Independent arguments in favour of long cloud lifetimes derive from observations of the Milky Way. Even the dusty, metal-enriched gas of the current Galactic disc converts to stars extremely slowly in the sense that less than one percent of a molecular cloud is turned into stars in a dynamical time. Moreover, since the overwhelming majority of the gas interior to the Sun is in molecular form, molecular clouds cannot be easily dissociated by star formation: their estimated lifetime is $\gtrsim 10^8$ yr (Scoville 2013).

Based on the above discussion, we expect clouds to orbit within the dark halo for several dynamical times before they are dissipated by stellar feedback. Thus we expect clouds to heat the halo for many dynamical times and to leave a DM-dominated galaxy when they are finally disrupted. However, it must be stressed that the lifetime of the clumps is a crucial parameter of the presented model and it would be highly desirable to obtain better constraints on it.

4 RELATION TO PREVIOUS WORK

In this paper we have shown that, before star formation, dwarf-galaxy sized cosmological halos are expected to host gaseous clumps with masses, sizes and orbits such that they quickly flatten the original DM cusp. The idea that massive clouds can effectively heat stellar systems dates back at least to Spitzer & Schwarzschild (1951). El Zant et al. (2001) proposed that a similar mechanism (baryonic clumps heating DM halos) could be responsible for turning DM cusps into cores. Subsequent work elaborated on this proposal, by considering specific applications to clusters of galaxies (El-Zant et al. 2004; Nipoti et al. 2004) or exploring the space of parameters by varying the density and velocity distribution of the host system and the clump mass, size and orbits (Arena & Bertin 2007; Jardel & Sellwood 2009; Goerdt et al. 2010; Cole et al. 2011). The results of these works clearly indicated, as a proof of concept, that dynamical friction heating by clumps can have an important role in halos on different scales and that, quantitatively, the relevance of this process depends on the properties of the clumps and of the host halo. However, not so much work has been done to quantify this effect specifically on the scale of dwarf galaxies. Here, though in an idealized framework, we try to estimate self-consistently the masses, sizes and orbits of the clumps and their effect on the DM distribution in a dwarf-sized halo of mass $\sim 10^9 M_\odot$. In this sense, among previous works, our investigation is most similar to that of Inoue & Saitoh (2011) who simulated, with a Smoothed Particle Hydrodynamics code, the formation of a disc galaxy in a relatively massive DM halo of $5 \times 10^{11} M_\odot$, finding significant evolution of the halo density profile due to interaction with baryonic clumps. However, these results cannot be extrapolated to the smaller scale of dwarf galaxies, because, as stressed above, a crucial quantity in the process is the ratio between the gas temperature at the time of fragmentation (set by quantum physics) and the virial temperature of the halo (set by gravity).

As an alternative to the mechanism considered in the present work, it has been suggested that the dominant factor in determining the final DM distribution is fluctuations of the gravitational potential that are driven by stellar feedback (e.g. Mashchenko et al. 2006, 2008). In such a scenario energy is transferred to the DM by the bulk motions of gas driven by repeated bursts of star formation. Though this scenario shares some features with the one considered in the present paper (gas clumps moving in the halo transfer energy to the DM), it must be stressed that the two scenarios are conceptually and materially different[1]: in one case the process occurs before star formation and the energy source is gravitational, in the other case the process occurs after star formation and the energy source is stellar feedback. The two mechanisms might be alternative or even cooperate during the formation and evolution of dSphs (see, for a discussion, Pontzen & Governato 2014). Remarkably, if the mechanism studied in our work is effective, it occurs before star formation and therefore earlier with respect to stellar-feedback driven processes. The effectiveness of the dynamical friction heating mechanism depends crucially on the lifetime of the clumps, which is a debated question. In Section 3 we have argued that, at least in the considered case of dwarf galaxies, the primordial clumps are expected to live long enough to erase the central DM cusp.

5 CONCLUSIONS

Dwarf spheroidal galaxies are now DM dominated, but stars cannot form until gas becomes locally gravitationally dominant. Dissipation causes gas to move inward within a DM halo until this condition is satisfied. When the mass of gas is small compared to the DM mass, considerable contraction is required to achieve gravitational dominance, and near-conservation of angular momentum will cause the gas distribution to become flattened. A differentially rotating body of gas will be heated by the processes that heat accretion discs, so its temperature will be much greater than that of the cosmic background radiation even in the case in which heating at the time of infall is extremely inefficient. In the absence of cooling by metal ions, it seems likely that, the temperature of the gas will rise to temperatures ~ 3000 K at which cooling by hydrogen becomes non-negligible, but we have considered also temperatures an order-of-magnitude lower.

In the potential of a low-mass halo, the disc may not be very thin, but equilibrium dynamical models of bodies of spinning gas moving in the common gravitational potential of the gas and DM suggest that it is probably thin enough for Toomre's seminal analysis of the stability of thin discs to yield the wavelength at which fragmentation first occurs to within a factor of a few. This wavelength in turn specifies the mass of the fragments into which the gas divides. The key point is that this mass is not very much smaller than the mass of DM interior to the radius where fragmentation starts. Consequently, only a few local dynamical times are required for the fragments to transfer significant energy to the local DM particles. Therefore the halo's central cusp is heated to form a core with central logarithmic density slope $\gamma \approx 0$ before stellar feedback enters the scene.

We have simulated this transfer with an N-body code, and find that it quickly erases the cusp at the centre of the original DM halo. This result is not at all surprising; the existence of DM cusps has

[1] The simulations of Mashchenko et al. (2006) are only superficially similar to those presented in Section 3: in their model, aimed at mimicking the gas bulk motions induced by successive episodes of stellar feedback, three massive clumps move as harmonic oscillators through the system's centre.

always been rather puzzling since they depend on the velocity dispersion within the halo decreasing to zero as one approaches the centre. Any gravitational scattering of the ultra-cool particles that form the cusp will raise the central velocity dispersion and erase the cusp. Hence the wonder is that such scattering does not occur during hierarchical merging of DM.

In a DM only simulation, the only objects capable of such scattering within a given halo are halos of smaller mass that reach the centre of the host halo. These halos have at their centres cusps that are dense, so are not tidally disrupted until the satellite halo has reached the very centre of it host (e.g. Binney & Tremaine 2008, section 9.3.2). It seems likely that cusp particles in the host halo that are upscattered by the satellite halo are efficiently replaced by the satellite halo's own cusp particles.

Gas can easily form clouds massive enough to scatter particles out of the host halo's cusp, and a gas cloud does not replace these particles. When the massive stars that form within the cloud disrupt it, the host halo is left DM dominated and in possession of a core.

This cusp erasing process will be efficient unless the gas cools to such low temperatures that it does not fragment until a *very* thin disc has formed. Since quantum physics sets the minimum temperature for efficient cooling, discs can be very thin at the onset of fragmentation only in higher-mass halos (which have higher virial temperatures). In these halos star formation is known to be more efficient in the sense that a greater fraction of gas is converted to stars before residual gas is returned to the intergalactic medium. In this case the stellar disc is likely to be self-gravitating, so it can become bar-unstable. A stellar bar quickly transfers energy to a co-spatial DM cusp (Tremaine & Weinberg 1984; Sellwood 2008), so spiral galaxies with bars will not have DM cusps either. In principle there might be an intermediate halo mass at which star formation is so inefficient that it leaves a completely DM dominated stellar disc, and yet at the onset of fragmentation the gas disc is sufficiently thin for the resulting gas clouds to be inefficient scatterers. Then in these intermediate-mass halos DM cusps would survive star formation. But the existence of this intermediate range of halo masses seems unlikely, so stars and DM cusps are probably mutually exclusive.

ACKNOWLEDGEMENTS

CN acknowledges financial support from PRIN MIUR 2010-2011, project "The Chemical and Dynamical Evolution of the Milky Way and Local Group Galaxies", prot. 2010LY5N2T. JB was supported by STFC by grants R22138/GA001 and ST/K00106X/1. The research leading to these results has received funding from the European Research Council under the European Union's Seventh Framework Programme (FP7/2007-2013) / ERC grant agreement no. 321067.

REFERENCES

Aaronson M., 1983, ApJ, 266, L11
Agnello A., Evans N. W., 2012, ApJ, 754, L39
Amorisco N. C., Agnello A., Evans N. W., 2013, MNRAS, 429, L89
Amorisco N. C., Zavala J., de Boer T. J. L., 2014, ApJ, 782, L39
Arena S. E., Bertin G., 2007, A&A, 463, 921
Arraki K. S., Klypin A., More S., Trujillo-Gomez S., 2014, MNRAS, 438, 1466
Assmann P., Fellhauer M., Wilkinson M. I., Smith R., 2013, MNRAS, 432, 274
Bournaud F., et al., 2014, ApJ, 780, 57
Battaglia G., Helmi A., Tolstoy E., Irwin M., Hill V., Jablonka P., 2008, ApJ, 681, L13
Battaglia G., Helmi A., Breddels M., 2013, NewAR, 57, 52
Binney J., 1977, ApJ, 215, 483
Binney J., Tremaine S., 2008, Galactic Dynamics 2nd Ed., Princeton University Press, Princeton
Birnboim Y., Dekel A., 2003, MNRAS, 345, 349
Blumenthal G. R., Faber S. M., Flores R., Primack J. R., 1986, ApJ, 301, 27
Breddels M. A., Helmi A., 2013, A&A, 558, A35
Ciotti L., Londrillo P., Nipoti C., 2006, ApJ, 640, 741
Cole D. R., Dehnen W., Wilkinson M. I., 2011, MNRAS, 416, 1118
Collins M. L. M., et al., 2014, ApJ, 783,
El-Zant A., Shlosman I., Hoffman Y., 2001, ApJ, 560, 636
El-Zant A. A., Hoffman Y., Primack J., Combes F., Shlosman I., 2004, ApJ, 607, L75
Faber S. M., Lin D. N. C., 1983, ApJ, 266, L17
Font A. S., et al., 2011, MNRAS, 417, 1260
Garrison-Kimmel S., Rocha M., Boylan-Kolchin M., Bullock J. S., Lally J., 2013, MNRAS, 433, 3539
Genel S., et al., 2012, ApJ, 745, 11
Goerdt T., Moore B., Read J. I., Stadel J., 2010, ApJ, 725, 1707
Governato F., et al., 2012, MNRAS, 422, 1231
Hopkins P. F., Quataert E., Murray N., 2012, MNRAS, 421, 3488
Inoue S., Saitoh T. R., 2011, MNRAS, 418, 2527
Ishiyama T., et al., 2013, ApJ, 767, 146
Jardel J. R., Sellwood J. A., 2009, ApJ, 691, 1300
Jardel J. R., Gebhardt K., Fabricius M. H., Drory N., Williams M. J., 2013, ApJ, 763, 91
Li Y.-S., De Lucia G., Helmi A., 2010, MNRAS, 401, 2036
Lin D. N. C., Faber S. M., 1983, ApJ, 266, L21
Loeb A., Furlanetto S. R., 2013, The First Galaxies in the Universe, Princeton University Press, Princeton
Londrillo P., Nipoti C., 2009, MSAIS, 13, 89
Londrillo P., Nipoti C., Ciotti L., 2003, MSAIS, 1, 18
Madau P., Shen S., Governato F., 2014, arXiv, arXiv:1405.2577
Mashchenko S., Couchman H. M. P., Wadsley J., 2006, Natur, 442, 539
Mashchenko S., Wadsley J., Couchman H. M. P., 2008, Sci, 319, 174
Mateo M. L., 1998, ARA&A, 36, 435
Mayer L., Governato F., Colpi M., Moore B., Quinn T., Wadsley J., Stadel J., Lake G., 2001, ApJ, 547, L123
Mayer L., Mastropietro C., Wadsley J., Stadel J., Moore B., 2006, MNRAS, 369, 1021
Milosavljević M., Bromm V., 2014, MNRAS, 440, 50
Muñoz-Cuartas J. C., Macciò A. V., Gottlöber S., Dutton A. A., 2011, MNRAS, 411, 584
Murray N., Quataert E., Thompson T. A., 2010, ApJ, 709, 191
Navarro J. F., Frenk C. S., White S. D. M., 1995, MNRAS, 275, 720 (NFW)
Navarro J. F., Eke V. R., Frenk C. S., 1996, MNRAS, 283, L72
Nipoti C., Londrillo P., Ciotti L., 2003, MNRAS, 342, 501
Nipoti C., Treu T., Ciotti L., Stiavelli M., 2004, MNRAS, 355, 1119
Ogiya G., Mori M., Ishiyama T., Burkert A., 2014, MNRAS, 440, L71

Peñarrubia J., Pontzen A., Walker M. G., Koposov S. E., 2012, ApJ, 759, L42
Pontzen A., Governato F., 2014, Natur, 506, 171
Prada F., Klypin A. A., Cuesta A. J., Betancort-Rijo J. E., Primack J., 2012, MNRAS, 423, 3018
Read J. I., Gilmore G., 2005, MNRAS, 356, 107
Revaz Y., et al., 2009, A&A, 501, 189
Romano D., Starkenburg E., 2013, MNRAS, 434, 471
Safronov V. S., 1960, AnAp, 23, 979
Sawala T., Scannapieco C., Maio U., White S., 2010, MNRAS, 402, 1599
Sawala T., Scannapieco C., White S., 2012, MNRAS, 420, 1714
Scoville N. Z., 2013, in Secular Evolution of Galaxies, J. Falcón-Barroso and J. H. Knapen eds., Cambridge University Press, Cambridge, 491
Sellwood J.A., 2008, ApJ, 679, 379
Simpson C. M., Bryan G. L., Johnston K. V., Smith B. D., Mac Low M.-M., Sharma S., Tumlinson J., 2013, MNRAS, 432, 1989
Spitzer L., Jr., Schwarzschild M., 1951, ApJ, 114, 385
Starkenburg E., et al., 2013, MNRAS, 429, 725
Stiavelli M., 2009, From First Light to Reionization: The End of the Dark Ages, Wiley-VCH, New York
Strigari L. E., Bullock J. S., Kaplinghat M., Simon J. D., Geha M., Willman B., Walker M. G., 2008, Natur, 454, 1096
Toomre A., 1964, ApJ, 139, 1217
Tremaine S., Weinberg M. D., 1984, MNRAS, 209, 729
Walker M. G., Peñarrubia J., 2011, ApJ, 742, 20
Walker M. G., Mateo M., Olszewski E. W., Peñarrubia J., Evans N. W., Gilmore G., 2009, ApJ, 704, 1274
Zolotov A., et al., 2012, ApJ, 761, 71